Physics in Medicine & Biology

Subset-dependent relaxation in block-iterative algorithms for image reconstruction in emission tomography

To cite this article: Eiichi Tanaka and Hiroyuki Kudo 2003 *Phys. Med. Biol.* **48** 1405

INSTITUTE OF PHYSICS PUBLISHING PHYSICS IN MEDICINE AND BIOLOGY

Phys. Med. Biol. **48** (2003) 1405–1422 PII: S0031-9155(03)55572-5

Subset-dependent relaxation in block-iterative algorithms for image reconstruction in emission tomography

Eiichi Tanaka[1] **and Hiroyuki Kudo**[2]

[1] Hamamatsu Photonics KK, Tokyo Branch, Mori-Bldg No 33, Minato-ku, Tokyo, Japan
[2] Institute of Information Sciences and Electronics, University of Tsukuba, Tsukuba-shi, Ibaraki, Japan

Received 5 November 2002, in final form 7 April 2003
Published 7 May 2003
Online at stacks.iop.org/PMB/48/1405

Abstract
This paper presents a row-action maximum likelihood algorithm (RAMLA), in which the relaxation parameter is controlled in such a way that the noise propagation from projection data to the reconstructed image is substantially independent of the access order of the input data (subsets) in each cycle of the sub-iterations. The 'subset-dependent' relaxation parameter $\lambda_k(q)$ is expressed as $\lambda_k(q) = \beta_0/(\beta_0 + q + \gamma k M)$, where M is the number of angular views, q $(0 \leqslant q \leqslant M - 1)$ is the access order of the angular view, k is the iteration number and β_0 and γ are constants. The constant β_0 deals with the balance of the noise propagation and the constant γ controls the convergence of iterations. The value of β_0 is determined from the geometrical correlation coefficients among lines of coincidence response. The proposed RAMLA using the subset-dependent (dynamic) relaxation 'dynamic RAMLA (DRAMA)' provides a reasonable signal-to-noise ratio with a satisfactory spatial resolution by a few iterations in the two-dimensional image reconstruction for PET. Dynamic OS-EM (DOSEM) has also been developed, which allows the use of a larger number of subsets (OS level) M_{sub} without loss of signal-to-noise ratio as compared to the conventional OS-EM. DRAMA is a special case of DOSEM, where $M_{\mathrm{sub}} = M$, and it is no more profitable to use DOSEM with a smaller M_{sub} $(<M)$, because DRAMA provides similar performance with the fastest convergence and smallest computer burden. This paper describes the theory, algorithm and the results of the simulation studies on the performance of DRAMA and DOSEM.

1. Introduction

Iterative statistical methods for image reconstruction in emission tomography have been widely studied since Shepp and Vardi (1982) published their paper on the expectation maximization

(EM) algorithm. To date, however, these methods have not been widely adopted for clinical use, mainly due to the slow convergence rate and the high overall computational cost. Several acceleration methods to reduce the computer burden have been proposed in the literature, and a recent trend is the use of block-iterative methods. In the ordered subsets (OS) EM algorithm (Hudson and Larkin 1994), projection data are grouped into a number of subsets, and the EM iterative procedure is repeatedly adopted for each subset until all subsets have been processed. The OS level is defined as the number of these subsets. A complete cycle of the successive sub-iterations for all subsets forms a main iteration of OS-EM. Each subset consists of projection views separated by some fixed angle about the object. In general, the larger the OS level the greater the acceleration that is achieved, and the convergence rate can be improved at least by an order of magnitude. The OS approach is not confined to EM. These include a number of Bayesian or penalized likelihood extensions of EM (Hebert and Leahy 1989, Green 1990, Levitan and Herman 1987). For example, the OS-GP algorithm is the OS extension of Green's one-step-late (OSL) algorithm (Hudson and Larkin 1994). Excessive acceleration by the use of a large OS level, however, results in the degradation in signal-to-noise ratio (Hudson and Larkin 1994, Meikle *et al* 1994). To overcome this drawback, Ogawa and Urabe (2000) proposed the modified OS-Bayesian reconstruction, in which the OS level is successively decreased, although it still needs several iterations to obtain reasonable images. Nevertheless, for the reconstruction of fully three-dimensional positron emission tomography (3D PET) data, OS-EM combined with the Fourier rebinning algorithm (FORE) (Defrise 1995) is now accepted as an attractive tool, where the 3D data are converted to a stack of 2D sinograms by FORE. The direct application of OS-EM to the 3D data has also been investigated (Xuan *et al* 2001).

A row-action maximum likelihood algorithm (RAMLA) has been proposed as a faster alternative to the EM algorithm for maximizing the Poisson likelihood in emission tomography (Browne and De Pierro 1996). In RAMLA, the reconstructed image is updated for each projection view (rows of the system matrix) in a controlled way using a relaxation parameter λ. Except for the existence of λ, RAMLA can be considered to be a special case of OS-EM where the OS level is equal to the number of projection views. Browne and De Pierro (1996) described a generalized RAMLA that utilizes the ordered subsets, which includes OS-EM as the special case. RAMLA uses a special ordering of the sequence of projection views to achieve a faster rate of convergence in a similar strategy to OS-EM. More recently, several authors reported block-iterative algorithms and discussed sufficient conditions for the global convergence. Kudo *et al* (1999, 2000) reported the block-gradient method that converges to the true solution for a class of cost functions. De Pierro and Yamagishi (2001) presented a block sequential regularized EM (BSREM) algorithm. They showed that, if the sequence generated by this method converges, then it must converge to the maximum *a posteriori* (MAP) solution based on the similar logic to that of RAMLA. Ahn and Fessler (2001) described the modified BSREM and the relaxed OS-SPS (ordered subsets separable paraboloidal surrogates), both of which are convergent to the true solution. Hsiao *et al* (2002a, 2002b) described an 'OS-EM'-like algorithm that uses a kind of built-in relaxation.

In general, λ is fixed throughout a complete cycle of sub-iterations, and a problem is that there has been no single choice for the 'relaxation sequence'. The optimal relaxation parameter depends on the particular task such as average structural accuracy, signal-to-noise ratio, hot or cold spot detectability, average log likelihood, etc. The appropriate parameter for a specific task can be selected by a training process (Browne and De Pierro 1996, Matej and Browne 1996, Obi *et al* 2000). In general, the use of a large λ allows a fast convergence when the data are consistent, but it tends to enhance the error due to inconsistent components (statistical noise) when the data contain the Poisson noise. This property prevents the use of

single iteration with a large λ, and several iterations are required with a small λ or with a successively decreasing λ. This is generally true for 2D reconstruction in PET. In the direct application of RAMLA to fully 3D PET data, on the other hand, the single iteration with a small λ may be feasible (Matej and Browne 1996, Daube-Witherspoon *et al* 2001) where the input data consist of a very large number of projection views and the image is updated for every view.

The undesirable feature on the noise enhancement with a large λ is due to the fact that the inconsistent components of data are propagated to the final image of the cycle of sub-iterations with different efficiency, and the final image contains more of the noise of the lately accessed views than those of the early views. The unbalanced propagation of the noise degrades the signal-to-noise ratio. This drawback will be improved by controlling the λ-value in the course of the sub-iterations in such a way that noise components of different views are propagated to the final image with a nearly equal efficiency. The main objective of this paper is to propose RAMLA using such a subset-dependent relaxation parameter, which provides sufficiently fast convergence with good signal-to-noise ratio. We call the algorithm 'dynamic RAMLA' or simply 'DRAMA' in this paper. The word 'dynamic' refers to the fact that the relaxation parameter changes during the sub-iterations. The same concept can also be applied to the other block-iterative algorithms such as OS-EM or OS-GP. With the 'dynamic OS-EM (DOSEM)', we can use a much larger OS level without degradation of the signal-to-noise ratio than the conventional OS-EM. The outline of this paper is the following: in the next section, we specify the iterative image reconstruction algorithms (DRAMA and DOSEM) used in the rest of the paper and the theory on the optimization of the dynamic relaxation parameter. In the following two sections, we describe the method and results of our simulation studies on the optimization of λ and on the imaging performance of DRAMA and DOSEM. In the last section, we describe a brief discussion of the consequences of our simulation studies and of our conclusions.

2. Theory

2.1. Iteration formula of dynamic RAMLA (DRAMA)

We consider the discretized 2D PET model. In the following, we assume that coincidence data are obtained along I lines of response (LORs) and denote by y_i $(1 \leqslant i \leqslant I)$ the number of detected coincidence events along the ith LOR. These data are arranged into M angular views with the view index m $(1 \leqslant m \leqslant M)$. Each view consists of N parallel LORs, where $I = M \times N$. We consider a square image matrix of $N \times N = J$ pixels, and photon emission from pixel j is denoted by x_j $(1 \leqslant j \leqslant J)$. Assuming that the image is updated sequentially for each projection view, the proposed DRAMA is expressed as follows:

$$x_j^{(k,0)} = x_j^{(k)} \tag{1.1}$$

$$x_j^{(k,q+1)} = x_j^{(k,q)} + \lambda_k(q)\frac{x_j^{(k,q)}}{C_j}\sum_{i\in S_q} a_{ij}\left(\frac{y_i}{\langle a^i, x^{(k,q)}\rangle} - 1\right) \tag{1.2}$$

where

$$C_j = \max_q \sum_{i\in S_q} a_{ij} \tag{1.3}$$

$$x_j^{(k+1)} = x_j^{(k,M-1)} \qquad \text{for } j = 1, 2, \ldots J, \quad q = 0, 1, 2, \ldots M-1, \quad k = 0, 1, 2, \ldots \tag{1.4}$$

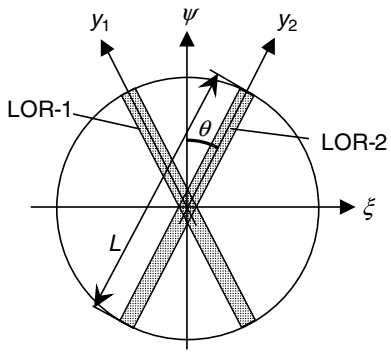

Figure 1. A model for geometrical correlation between two LORs.

where a_{ij} is the probability that a photon emission from pixel j is recorded in the ith LOR, $\langle a^i, x\rangle = \sum_{j=1}^{J} a_{ij}x_j$ denotes the forward projection along the ith LOR, q is the index of the access order of views and S_q is the set of LORs ($m(q)$th angular view) accessed at qth order. The index k refers to the main iterations, each of which corresponds to a complete cycle of M sub-iterations using all input data, $\lambda_k(q)$ is the relaxation parameter ($0 < \lambda_k(q) \leqslant 1$) and C_j is the normalization matrix. We assume that the iteration starts with a positive image ${x_j}^{(0)} > 0$. The view index $m(q)$ is the permutation of the access order q, the two indices being related by an ordering method described later. To regularize the reconstructed image, we apply the post-smoothing with a Gaussian filter after the iterations are terminated (Snyder and Miller 1985).

We modified the iterative formula such that the normalization factor C_j is dependent on the pixel j. This modification would help to accelerate the convergence in particular for the case where the attenuation factor (averaged with respect to all angles) largely depends on the pixel j because the pixel-dependence of the attenuation factor can be normalized by C_j at each iteration. The rationale behind this modification is as follows: one of the key ideas of RAMLA is to use the constant normalization factor $C_j = \text{constant} = \max_{q,j} \sum_{i\in S_q} a_{ij}$ to avoid the convergence to an incorrect (weighted Kuhn–Tucker) solution (appendix B of Browne and De Pierro 1996). This good property seems to be still valid even if the normalization factor C_j is dependent on the pixel j (but it is not valid anymore if C_j is dependent on q in the form of C_{jq}).

2.2. Noise propagation and dynamic relaxation parameter (DRP)

We now discuss the propagation of noise from projections to the final image of a main iteration, and define the dynamic relaxation parameter (DRP) $\lambda_k(q)$. We assume that attenuation of photons is negligibly small or the projection data are pre-corrected for attenuation in this section. Suppose a simplified model shown in figure 1, where we assume that projections y_1 and y_2 are accessed at orders q_1 and q_2 ($>q_1$) along LOR-1 and LOR-2, respectively. The view indices of LOR-1 and LOR-2 are related to q_1 and q_2, respectively, by a permutation $m(q)$ determined by an access ordering method described later. We denote by $\lambda(q_1)$ and $\lambda(q_2)$ the respective relaxation parameters. We drop here the subscript k for simplicity, and consider only a single main iteration. We assume that projection y_1 has Poisson statistical noise, while the projection y_2 is noiseless. The noise component of y_1 yields an error in the image density along LOR-1 proportional to $\lambda(q_1)$. The error will be modified by the following correction process for the other views at different angles. An analysis (see appendix A) shows that the noise component of y_1 is reduced approximately by a factor of $\lambda(q_1)\{1 - \lambda(q_2)g^2(q_1, q_2)\}$

after processing y_2, where $g(q_1, q_2)$ is the geometrical correlation coefficient between the two LORs. Then, the noise component of any projection y accessed at qth order will appear in the final image of the complete cycle of the sub-iterations with a propagation efficiency given by

$$\varepsilon(q) = \lambda(q) \prod_{r=q+1}^{M-1} \{1 - \lambda(r) g^2(q, r)\}. \tag{2}$$

The geometrical correlation coefficient $g(q_1, q_2)$ is defined as

$$g(q_1, q_2) = \sum_{j=1}^{J} a_{1j} a_{2j} \Bigg/ \left[\sum_{j=1}^{J} a_{1j}^2 \sum_{j=1}^{J} a_{2j}^2 \right]^{1/2}. \tag{3}$$

In the practical algorithm, the reconstructed image is regularized by post-smoothing as described before. The post-smoothing increases the geometrical correlation coefficient, as if the system matrix includes the smoothing effect, even though the iteration is performed without any smoothing. Therefore, when the geometrical correlation $g(q_1, q_2)$ is evaluated, the system matrix a_{ij} in equation (3) should include the response of the post-smoothing. In practice, $g(q_1, q_2)$ is calculated assuming that LORs have a Gaussian cross section corresponding to the post-smoothing (see appendix B). Since the image is updated for each projection view S_q, the correlation coefficient has to be averaged over all combinations of two LORs (i_1, i_2) such that $i_1 \in S_{q_1}$ and $i_2 \in S_{q_2}$.

Our intention is now to find $\lambda(q)$ that yields a constant $\varepsilon(q)$ defined by equation (2). We refer to such $\lambda(q)$ as the optimized dynamic relaxation parameter (ODRP). If $m(q)$ and $g(q, r)$ are known, it is not difficult to obtain the ODRP by an iterative method based on equation (2) as described later. However, if we can replace $g^2(q, r)$ in equation (2) by its average value $1/\beta_0$ defined by

$$\frac{1}{\beta_0} = \frac{1}{M-1} \sum_{\Delta m=1}^{M-1} g^2(\Delta m) \tag{4}$$

we can derive a simple analytical expression for the ODRP given by

$$\lambda(q) = \beta_0/(\beta_0 + q) \tag{5}$$

because we have, from equations (2), (4) and (5)

$$\begin{aligned} \varepsilon(q) = \lambda(q) \prod_{r=q+1}^{M-1} \left\{ 1 - \frac{\lambda(r)}{\beta_0} \right\} &= \frac{\beta_0}{\beta_0 + q} \prod_{r=q+1}^{M-1} \frac{\beta_0 + (r-1)}{\beta_0 + r} \\ &= \beta_0/(\beta_0 + M - 1) \qquad (= \text{constant}). \end{aligned} \tag{6}$$

We estimated the geometrical correlation coefficient $g(\Delta m)$ assuming the two LORs model shown in figure 1, where the LORs have a cross-sectional response representing the Gaussian post-smoothing. The coefficient is given by (see appendix B for the derivation):

$$g(\Delta m) = \frac{2}{L \cos\theta} \int_0^{L/2} \exp\left\{ -\frac{(\psi \sin\theta)^2}{\sigma^2} \right\} \mathrm{d}\psi \qquad (0 \leqslant \Delta m \leqslant M/2 \text{ and } \sin\theta \leqslant 3\sqrt{2}\,\sigma/L) \tag{7.1}$$

$$= 2\sqrt{\pi}\,\sigma/\{L \sin(2\theta)\} \qquad (0 \leqslant \Delta m \leqslant M/2 \text{ and } \sin\theta > 3\sqrt{2}\,\sigma/L) \tag{7.2}$$

$$= g(M - \Delta m) \qquad (M/2 < \Delta m \leqslant M - 1) \tag{7.3}$$

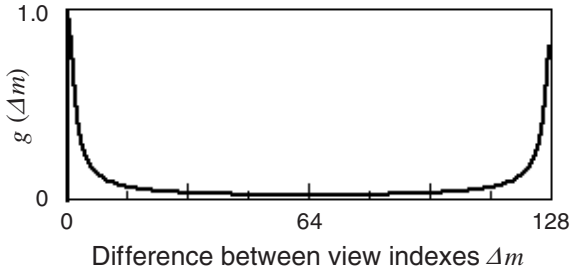

Figure 2. Geometrical correlation coefficient. $M = N = 128$, $s_{\mathrm{FWHM}} = 2.0$ pixels.

where $2\theta = \pi\Delta m/M$ is the angle between the two views, $\sigma = \mathrm{FWHM}/2.355$ (FWHM is the full-width at half-maximum) is the standard deviation of the Gaussian kernel of the post-smoothing and L is the length of LORs intersecting the field of view. Figure 2 shows an example of the calculated correlation coefficient assuming that $M = N = 128$, $L = 128$ (pixels), and FWHM of the Gaussian kernel is 2.0 (pixels).

To control the convergence of the main iterations, we modify the ODRP to include another parameter γ as follows:

$$\lambda_k(q) = \beta_0/(\beta_0 + q + \gamma k M) \qquad (0 \leqslant \gamma \leqslant 1). \tag{8}$$

Equation (8) was derived so as to yield balanced noise-propagation in each cycle of sub-iterations. In fact, from equations (2), (4) and (8), we obtain $\varepsilon(q) = \beta_0/(\beta_0 + M - 1 + \gamma k M)$, which shows that $\varepsilon(q)$ is independent of q. We now consider the convergence of our algorithm intuitively. It is likely that if the relaxation sequence has the form $c_1/(c_2 + k)$, where c_1 and c_2 are constants, the algorithm converges to the true solution (Kudo *et al* 1999, 2000, Ahn and Fessler 2001), although the theoretical investigation is necessary because the above iteration formula is not exactly the same as those in Kudo (1999, 2000) and Ahn and Fessler (2001). Equation (8) is rewritten in the form $\lambda_k(q) = A/\{B(q) + k\}$, where $A = \beta_0/(\gamma M)$ is a constant and $B(q) = (\beta_0 + q)/(\gamma M)$ is a function of q. During the cycle of sub-iterations of the kth main iteration, $\lambda_k(q)$ decreases with q, and the maximum change of $\lambda_k(q)$ in the cycle is given by $\Delta\lambda_k = \lambda_k(0) - \lambda_k(M - 1)$. We can easily show that, as k increases, $\Delta\lambda_k$ approaches zero with a speed $O(1/k^2)$, while $\lambda_k(q)$ diminishes with $O(1/k)$. In other words, we can neglect the change of $B(q)$ during the cycle of sub-iterations for a sufficiently large k. Therefore we can expect intuitively that the algorithm is globally convergent to the true solution for ${x_j}^{(0)} > 0$. The rigorous theoretical issue on the convergence is beyond the scope of this paper.

The speed of convergence will be controlled by choosing γ. If we set $\gamma = 0$, the value of $\lambda_k(q)$ is renewed at the start of each main iteration, and the ODRP is given by equation (5) independently of k. The convergence rate is highest, but we may have a risk of convergence to a limit cycle, which is different from the true solution, due to the inaccuracy in the balance of the noise propagation. When $\gamma = 1$, on the other hand, the value of $\lambda_k(q)$ continues to decrease and the limit cycle can be eliminated, but the convergence is slow. We expect that the intermediate value will give a reasonable speed of convergence without a risk of convergence to a limit cycle.

2.3. Dynamic OS-EM (DOSEM)

In DOSEM, M angular projection views are grouped into M_{sub} subsets, each consisting of M/M_{sub} views, where M_{sub} is the OS level. The iteration formula for DOSEM is again

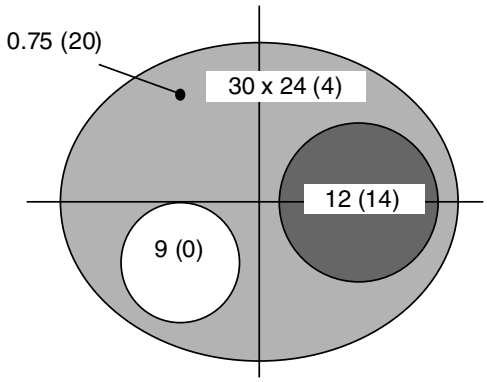

Figure 3. Phantom for testing structural recovery. Numerals are the diameters (cm) and the relative activities (parentheses).

expressed by equation (1) except that the access order index q ranges from 0 to $M_{\text{sub}} - 1$, and S_q is the set of LORs involved in the subset accessed at qth order. The geometrical correlation coefficient $g(q_1, q_2)$ between the two data accessed at different orders is given by the average of the correlation coefficients for all combinations of two LORs (i_1, i_2) such that $i_1 \in S_{q_1}$ and $i_2 \in S_{q_2}$. Then, the ODRP is also given by equations (5) or (8) independently of M_{sub}. DRAMA is a special case of DOSEM, where $M_{\text{sub}} = M$.

3. Method of simulation studies

3.1. General descriptions

We performed simulation studies employing computer generated projection data using mathematical phantoms. The projection data were obtained by forward projection of the phantom image, assuming that the activity is uniform in the rectangular pixels. The projection data were arranged into M angular views, each view consisting of N parallel LORs. We controlled the spatial resolution by post-smoothing with a Gaussian filter, the FWHM of which was expressed as s_{FWHM} (pixels). Figure 3 shows the phantom that was used for testing the structural recovery of the reconstruction. It consists of an elliptic uniform disc, a circular hot area, a cold area and a sharp spot. The diameters and the relative activities of the elements are shown in the figure. The size of the image matrix is 384 × 384 (mm). For comparison, we reconstructed images with the filtered backprojection (FBP) method. In the FBP, we used a ramp filter, and the obtained image was smoothed with a Gaussian filter (post-smoothing) to control the spatial resolution.

We evaluated the performance of algorithms by the following four items.

- *Structural error* (*SE*). This item measures how the reconstructed image is close to the phantom image. The value *SE* was calculated by taking the average of the absolute difference between reconstructed pixel values and the phantom over the whole region of interest, and expressed as the ratio to the mean density of the phantom. For this test, we used the phantom shown in figure 3, and we smoothed the phantom with the same filter as that used in the post-smoothing for the reconstructed image. Statistical noise was not added in this test. Since the phantom has a cold area of zero-activity, the value of *SE* is sensitive to the recovery of the border of the cold area and does not represent the structural accuracy of the whole image.

- *Spatial resolution* (R_{FWHM}). We first generated the projection data of a uniform disc phantom, and then we added a constant value to the pixels along a LOR to simulate a line source (one pixel width) embedded in the phantom. We defined R_{FWHM} as the FWHM of the line-spread function of the reconstructed image evaluated by fitting it with a Gaussian function. The value was expressed in terms of pixels.
- *RMS noise* (N_{RMS}). Root mean square (RMS) noise of the reconstructed image was evaluated with a uniform circular disc phantom. The value was calculated by taking the average of the squared difference between reconstructed pixel values and its true values over the central circular region having 80% of the phantom in diameter.
- *Noise equivalent* (N_{equiv}). We defined N_{equiv} as the RMS noise normalized by that of the FBP image having a spatial resolution R_{FWHM} equivalent to the image under test:

$$N_{\mathrm{equiv}} = \frac{N_{\mathrm{RMS}} \text{ of the test image}}{N_{\mathrm{RMS}} \text{ of FBP image having equivalent } R_{\mathrm{FWHM}}}. \tag{9}$$

  Note that, since the normalization is performed using data of a disc phantom, N_{equiv} is not affected by the non-negativity of the reconstruction algorithm. The N_{equiv} value greater than unity may imply the excessive noise, while a smaller value less than unity will imply insufficient recovery of the spatial resolution.

3.2. Access order of projection data

In RAMLA, it is preferable to adjust the access order in such a way that projection views at angles far apart are updated consecutively to keep the geometric correlation small (Herman and Meyer 1993, Guan and Gordon 1994). We have tested three methods for the access ordering. The first one is the method of the multilevel scheme (MLS) proposed by Guan and Gordon (1994). The access order is that for the 1D FFT (bit reversal) and the method is easy to implement if the number of projection views is a power of two. Herman and Meyer (1993) proposed a similar method. The second method is a constant increment scheme (CIS) based on the following recursive formula:

$$m(q+1) = (m(q) + \text{constant}) \bmod M + 1 \tag{10}$$

where $m(q)$ is the view number accessed at qth order. The 'constant' in equation (10) was determined empirically as the integer number nearest to but not larger than $M/2.7$. The third method is a random permutation scheme (RPS) generated by

$$m(q+1) = (m(q) + \text{random number}) \bmod M + 1. \tag{11}$$

In the latter two methods, if $m(q+1)$ is already used, the value is increased by 1 until obtaining a new value.

4. Results of simulation studies

4.1. Optimized dynamic relaxation parameter (ODRP)

The optimal value β_0 defined by equation (4) is a function of M, N, L and σ in equation (7). The typical values are listed in table 1, where we assumed that $L = N$ (pixels) and $\sigma = \sqrt{s_{\mathrm{FWHM}}^2 + 1.0}/2.355$, where s_{FWHM} is the FWHM of the Gaussian post-smoothing. The value 1.0 in the square-root mark was inserted to deal with the case of no post-smoothing. Note that β_0 is approximately proportional to M (when $M = N$) and $1/s_{\mathrm{FWHM}}$.

The ODRP $\lambda(q)$ obtained with the three access ordering methods is shown in the top row of figure 4, where $M = N = 128$ and $s_{\mathrm{FWHM}} = 2.0$ (pixels). The smooth curves (same for all cases) in the figures are the simple ODRP expressed by equation (5), and the zigzag curves are

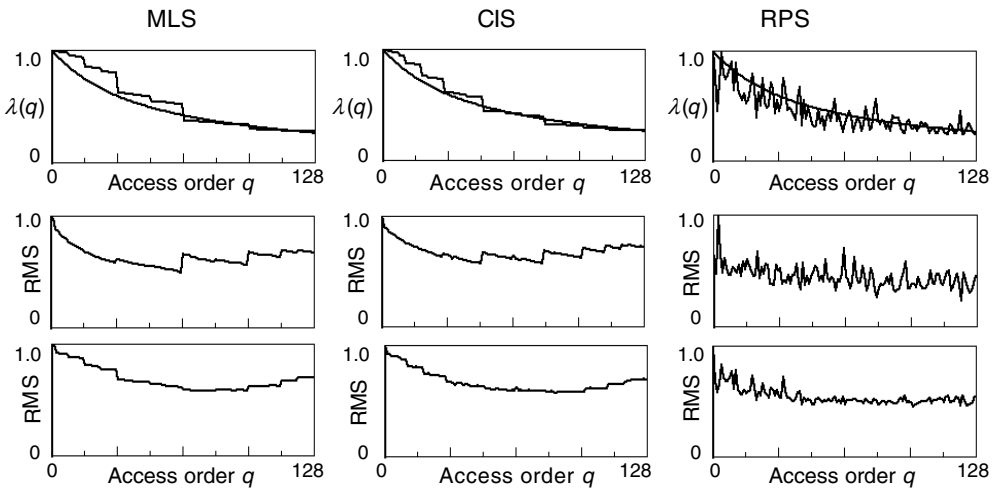

Figure 4. ODRP $\lambda(q)$ (top row) and noise propagation as a function of access order. Top row: smooth and zigzag curves are simple and exact ODRPs, respectively. Second row: RMS noise propagation with the simple ODRP. Third row: RMS noise propagation with the exact ODRP.

Table 1. Optimal values β_0 for various imaging conditions.

M	128	128	128	128	256	256	256	256
N	128	128	128	192	192	256	256	256
s_{FWHM} (pixels)	1.0	2.0	3.0	2.0	2.0	1.0	3.0	5.0
β_0	92.7	46.5	29.7	84.6	63.8	184.3	59.2	33.7

the ODRP given by an exact solution based on equation (2) (computed by an iterative method). We performed the following test to observe how the statistical noise of an angular view is propagated to the final image of each main iteration cycle. We first prepared a set of noiseless projection data assuming a uniform disc phantom. Next, we added Poisson noise only to the projection view accessed at qth order (others were kept noiseless), and we reconstructed the image and evaluated the RMS noise at the end of the main iteration cycle. We repeated the test changing the access order q of the noisy view in the range from 0 to $M - 1$. The relative RMS noise (normalized by the maximum value) is plotted in the second and third rows of figure 4 as a function of access order q. The second row shows the noise propagation with the simple ODRP, and the third row shows that with the exact ODRP by iteration. It is seen that the stepwise changes in the curves with the simple ODRP are removed in the curves with the exact ODRP, but the obtained noise propagation curves are not so flat as expected for both the ODRPs. The reason for this observation may partly be unreasonable approximations involved in deriving the ODRP, but another reason will be that the iterative correction process is not only non-linear but also its frequency response is not uniform. The image updating is more effective for the lower frequency component than for higher frequency component in the EM algorithm (Tanaka 1987). (We confirmed by simulation that the image of an impulse noise added to a projection is gradually differentiated as the iteration proceeds.) As a result, the high frequency component of noise will not decrease as expected from equation (2).

We compared the reconstructed images with the three access orderings using the simple ODRP. The computation was terminated after a single main iteration (after all input data were accessed only once). The difference between the two permutations, MLS and CIS, was not meaningful, but RPS was apparently inferior to the others. Structural error SE was 1.64% with

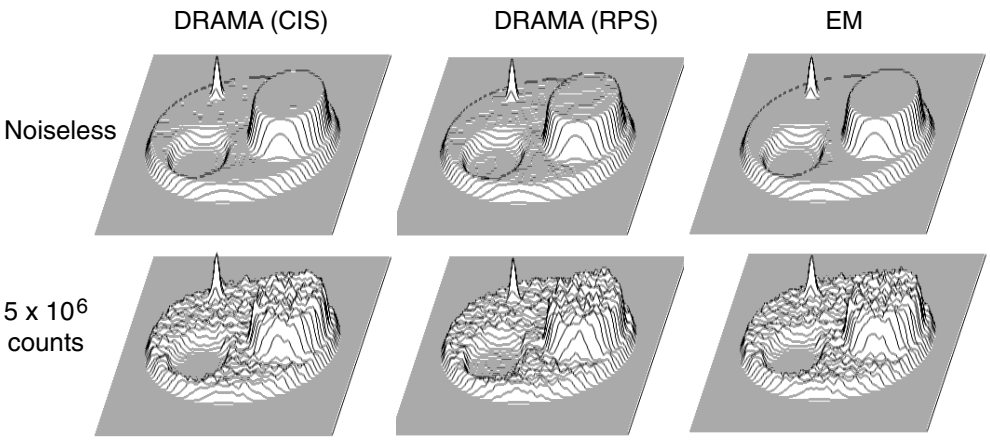

Figure 5. Comparison of DRAMA ($n_{\mathrm{iter}} = 1$) with two permutations, CIS and RPS, and EM algorithm ($n_{\mathrm{iter}} = 100$). $M = N = 128$, $s_{\mathrm{FWHM}} = 2.0$ pixels and the total counts (lower row) $= 5 \times 10^6$.

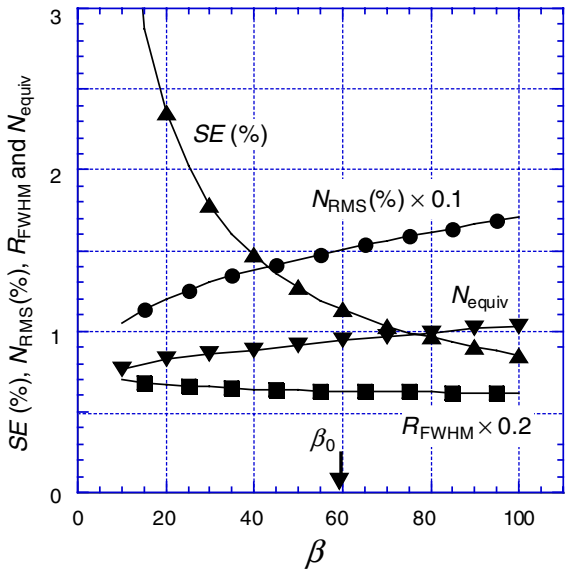

Figure 6. Performance of DRAMA with various β: $M = N = 256$ and $s_{\mathrm{FWHM}} = 3.0$ pixels.

CIS while 2.73% with RPS. Figure 5 shows the images of the phantom reconstructed with CIS and RPS, and that obtained with the EM algorithm (100 iterations) for comparison. We did not find any meaningful improvement by the use of exact ODRP instead of the simple ODRP. Hence, in the following studies, we used CIS permutation and the simple ODRP.

4.2. Performance of dynamic RAMLA (DRAMA)

The main feature of DRAMA is the use of ODRP $\lambda(q)$ expressed by equations (5) or (8). Before optimizing the value of β_0, we tested the performance of DRAMA of single iteration with the DRP, $\lambda(q) = \beta/(\beta + q)$, for various β-values. The results obtained with $M = N = 256$ and $s_{\mathrm{FWHM}} = 3.0$ (pixels) are shown in figure 6. Noise tests were performed with the

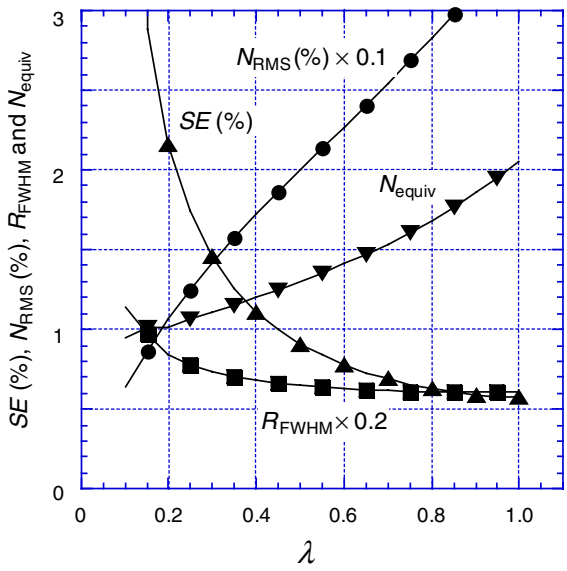

Figure 7. Performance of RAMLA with various constant λ: $M = N = 256$ and $s_{FWHM} = 3.0$ pixels.

total count of 1×10^7. Attenuation and scattering of photons were ignored. It is shown that the performance is relatively insensitive to the value of β, and DRAMA provides satisfactory performance in a range $40 < \beta < 100$. The optimum value of β_0 determined by equation (4) was 59.5 (shown by an arrow in the figure). Similar data obtained with various fixed relaxation parameters are shown in figure 7. It is seen that the performance is quite sensitive to the value of λ, and that reasonable noise is attained at $\lambda < 0.2$, while R_{FWHM} has reasonable values in a range $\lambda > 0.4$. In other words, there is no λ-value that yields satisfactory performance for the structural recovery, noise performance and reasonable spatial resolution simultaneously. Note that N_{equiv} is larger than unity for the range $\lambda > 0.2$, which implies excess noise. A similar test was performed with the EM algorithm. Figure 8 shows the results of the EM algorithm (solid symbols) and those of DRAMA (open symbols) as a function of iteration number. The data on DRAMA were obtained with the ODRP and $\gamma = 0$. We see that a single iteration of DRAMA is equivalent to the EM algorithm with the iteration numbers of about 105 for *SE*, 220 for R_{FWHM} and 170 for N_{RMS}.

Figure 9 shows the results of an example of multiple iterations obtained with the two extremes, the renewal mode ($\gamma = 0$) and the continual mode ($\gamma = 1$), with $M = 128$, $N = 256$, $s_{FWHM} = 3.0$ (pixels) and $n_{iter} = 3$. It is shown that, in the renewal mode, N_{RMS} increases appreciably at the middle of each main iteration because the noise propagation is balanced only at the end of each main iteration. In the continual mode, on the other hand, the noise propagation is nearly balanced throughout the course of each main iteration, and hence we can terminate the iteration even in the middle of a cycle of the sub-iterations without losing signal-to-noise ratio.

We compared the behaviour of main iterations of DRAMA with those of RAMLA and EM algorithm. In RAMLA, we temporarily assumed that the relaxation parameter is given by $\lambda_k = 0.48c/(c+k)$ ($k = 0, 1, 2, \ldots$), where c is a constant. The factor 0.48 is equal to the mean value of $\lambda_k(q)$ for $q = 0$–127 ($k = 0$), with which RAMLA yields a *SE* value nearly equal to that of DRAMA with a single iteration. Figure 10 shows the plots of N_{RMS} versus *SE*

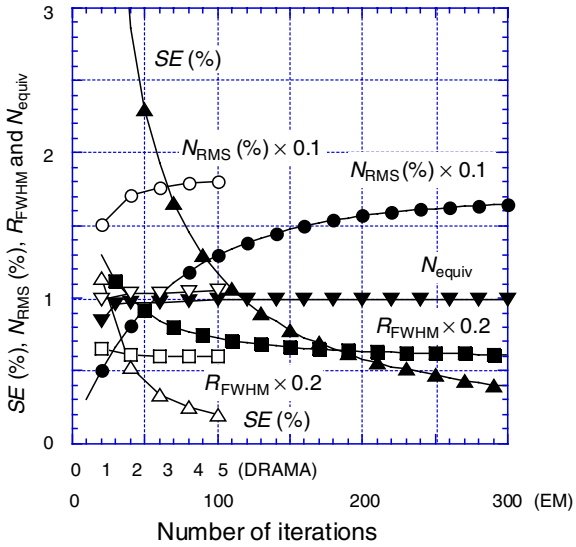

Figure 8. Comparison between EM algorithm (solid symbols) and DRAMA with ODRP and $\gamma = 0$ (open symbols): $M = N = 256$ and $s_{\mathrm{FWHM}} = 3.0$ pixels.

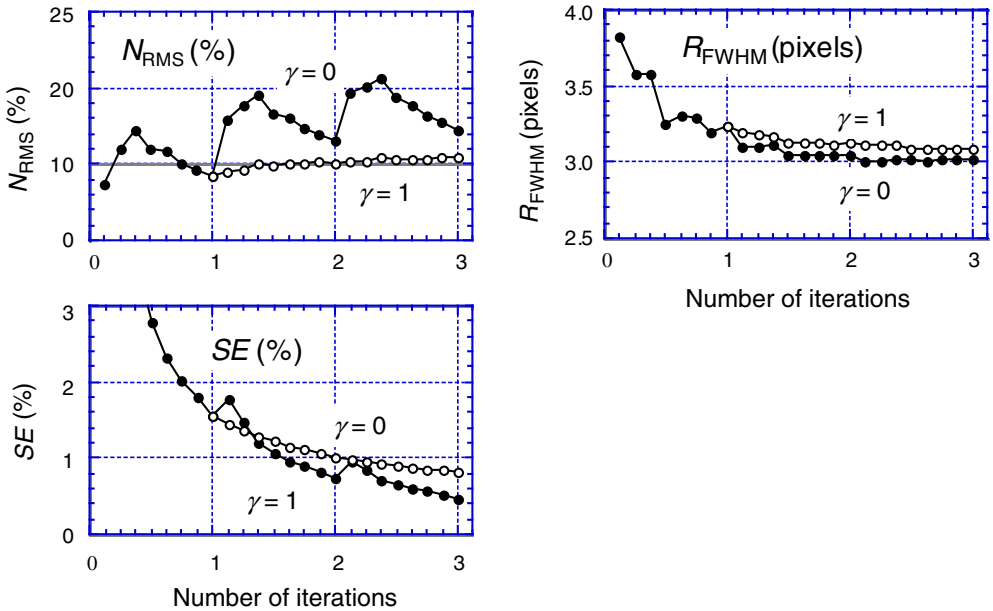

Figure 9. Comparison between renewal ($\gamma = 0$) and continual ($\gamma = 1$) modes on the main iterations: $M = 128$, $N = 256$, $s_{\mathrm{FWHM}} = 3.0$ pixels.

(upper left), R_{FWHM} versus SE (upper right) and N_{RMS} versus R_{FWHM} (bottom). We see that the plots of DRAMA ($\gamma = 0.1$) and RAMLA ($c = 5$ or 2.5) approach those of the EM algorithm as the iteration proceeds. It is also shown that DRAMA is superior to RAMLA in both of N_{RMS} and R_{FWHM} for a given SE or n_{iter} (<5). It is worth noting that, in the N_{RMS}–R_{FWHM}

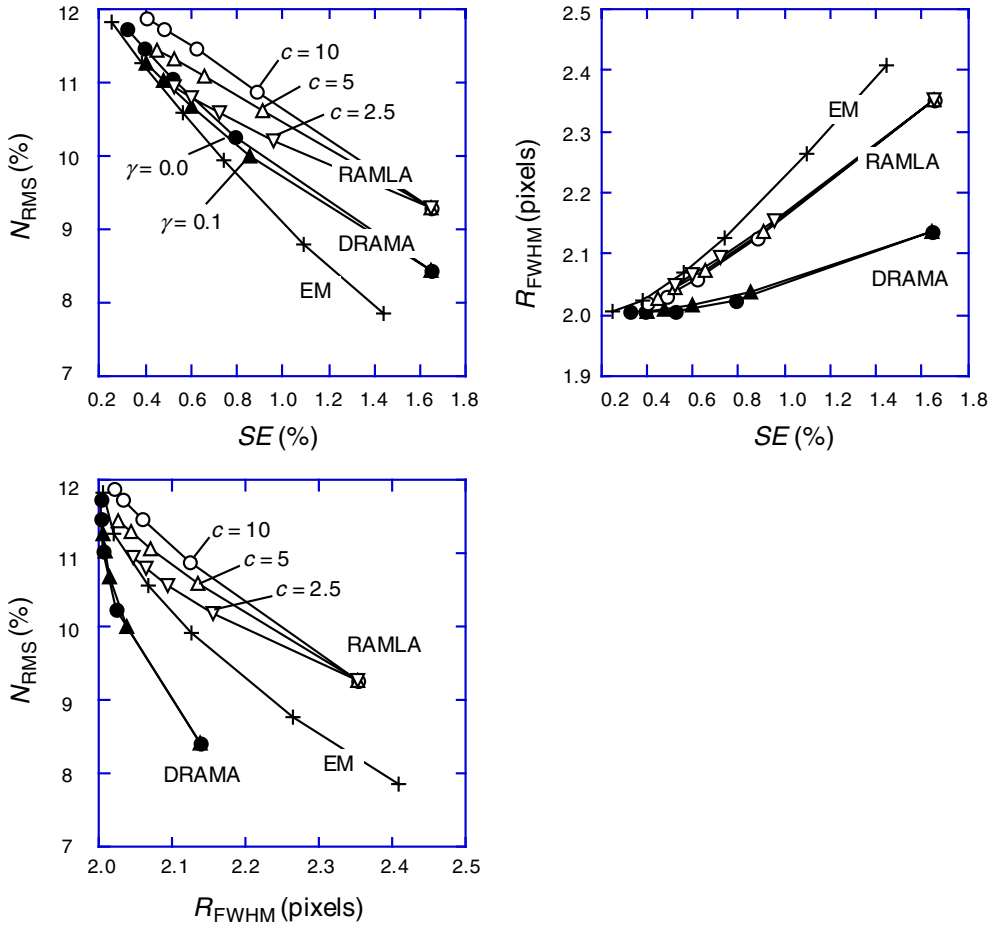

Figure 10. Plots of N_{RMS} versus SE (upper left), R_{FWHM} versus SE (upper right) and N_{RMS} versus R_{FWHM} (bottom). $M = N = 128$, $s_{FWHM} = 2.0$ pixels and total counts $= 1 \times 10^7$. Solid symbols are DRAMA with 1, 2, 3, 4 and 5 iterations, open symbols are RAMLA with 1, 2, 3, 4 and 5 iterations and crosses are EM algorithm with 75, 100, 150, 200, 300 and 500 iterations.

relation (bottom figure), the plots of DRAMA approach to the EM curve from the lower noise (or higher resolution) side, while the plots of RAMLA do so from the opposite side.

4.3. Performance of dynamic OS-EM (DOSEM)

We performed comparative simulation studies on DOSEM and the conventional OS-EM. Table 2 shows the results obtained with $M = N = 256$, and $s_{FWHM} = 3.0$ (pixels). The number of main iterations n_{iter} was chosen in such a way that the total number of sub-iterations was 256. The iteration was performed with the renewal mode. N_{RMS} and N_{equiv} increased with increasing M_{sub} in the conventional OS-EM, while these values were nearly independent of M_{sub} in DOSEM as expected.

We now define T_u as the sum of $\lambda(q)$ over a cycle of sub-iterations ($\gamma = 0$):

$$T_u = \sum_q \lambda(q) \qquad (0 \leqslant q \leqslant M_{sub} - 1). \tag{12}$$

Table 2. Comparison of DRAMA, DOSEM, OS-EM and EM ($M = N = 256$, $s_{\mathrm{FWHM}} = 3.0$ pixels).

	M_{sub}	n_{iter}	SE (%)	R_{FWHM} (in pixels)	N_{RMS} (%)	N_{equiv}	T_{u}	$SE \times T_{\mathrm{u}} \times n_{\mathrm{iter}}$
DRAMA	256	1	1.141	3.15	15.02	0.940	99.4	113
DOSEM	128	2	0.825	3.18	15.26	0.968	68.5	113
	64	4	0.658	3.15	15.72	0.984	43.7	115
	32	8	0.583	3.14	15.93	0.992	25.8	120
	16	16	0.511	3.11	16.08	0.988	14.3	113
OS-EM	128	2	0.475	3.05	21.63	1.292	128	122
	64	4	0.466	3.08	17.71	1.073	64	119
	32	8	0.494	3.09	16.58	1.009	32	126
	16	16	0.458	3.09	16.37	0.996	16	117
EM	1	256	0.459	3.10	16.22	0.992	1	118

Since each image updating is performed in proportion to $\lambda(q)$, T_{u} implies the effective time of image updating through one cycle of the sub-iterations. The values of T_{u} and $SE \times T_{\mathrm{u}} \times n_{\mathrm{iter}}$ are listed in table 2 . Note that the values of $SE \times T_{\mathrm{u}} \times n_{\mathrm{iter}}$ are fairly constant for all cases. This implies that the structural recovery is proportional to $T_{\mathrm{u}} \times n_{\mathrm{iter}}$ and DOSEM needs a little larger n_{iter} than OS-EM to achieve the same SE. In other words, we can say that the signal-to-noise ratio is guaranteed in DOSEM even for a large OS level at a certain sacrifice of structural recovery or at the cost of convergence speed.

4.4. Attenuation correction

In the attenuation correction in PET imaging, we have two fundamental schemes. The one is 'attenuation pre-correction scheme (APCS)', in which the projection data are pre-corrected for attenuation and the image reconstruction is performed without attenuation correction. The other is 'weighted attenuation correction scheme (WACS)', where attenuation correction is incorporated in an iterative image reconstruction algorithm. For FORE + OS-EM in 3D PET, we first pre-correct the 3D projection data for attenuation prior to FORE, and we usually apply APCS. In this scheme, the 2D sinograms rebinned by FORE deviate greatly from Poisson statistics, and are inadequate for iterative algorithms based on Poisson statistics. Comtat *et al* (1998) showed that WACS using OS-EM improved noise-bias trade-off relative to the APCS. To apply the WACS in FORE + OS-EM, we multiply the attenuation factors to the rebinned 2D singrams to restore the Poisson-like statistics to the data, and then apply the WACS.

We checked the performance of DRAMA for the two schemes in comparison with the conventional OS-EM (OS level = 8). We assumed a circular disc phantom of 30 cm in diameter having a uniform activity density for this test. The attenuation coefficient is $0.0958\ \mathrm{cm}^{-1}$ except an elliptic area of no-attenuation. The elliptic area has major diameters of 12 cm (x-direction) and 21 cm (y-direction) and is located 4 cm off-centre in the x-direction. The matrix size N and number of views M were 128. The total number of counts was 1×10^7. We evaluated the RMS noise N_{RMS} and the uniformity (average of the absolute difference from the mean) of the reconstructed image in the concentric circular area having 24 cm in diameter. The reconstructed images were post-smoothed so as to yield the same spatial resolution $R_{\mathrm{FWHM}} = 2.0$ (pixels). Table 3 shows the results. We saw a clear improvement in the signal-to-noise ratio by using the WACS instead of the APCS in DRAMA as well as in OS-EM.

Table 3. Performance of DRAMA and OS-EM for attenuation correction.

Scheme	Algorithm	Parameters	n_{iter}	N_{RMS} (%)	Uniformity (%)
APCS	OS-EM	OS level = 8	16	12.51	0.056
	DRAMA	$\gamma = 0$	2	12.56	0.060
WACS	OS-EM	OS level = 8	16	11.01	0.077
	DRAMA	$\gamma = 0$	3	10.69	0.115

Table 4. Effect of s_{FWHM} on the structural error SE ($M = N = 256$, $n_{\text{iter}} = 1$).

s_{FWHM} (pixels)	1.0	2.0	3.0	4.0	5.0
β_0	184	92.6	59.2	43.1	33.7
T_{u}	161	123	99.4	83.9	72.9
SE (%)	1.15	1.07	1.14	1.21	1.26

5. Discussion and conclusions

We have proposed new block-iterative algorithms incorporating the optimized dynamic relaxation parameter (ODRP), which controls the image updating of RAMLA in such a way that the noise propagation from projection data to the final image is independent of the data access order in each cycle of sub-iterations. The resultant algorithm DRAMA can provide a reasonable signal-to-noise ratio with a satisfactory spatial resolution by a few iterations. We expect intuitively that the algorithm is globally convergent to the true solution if we use a suitable value of γ. The experimental results shown in figure 10 seem to support our expectation on the convergence.

The key parameter of the algorithm is the constant β_0 in equations (5) and (8). The optimum value of β_0 is affected by the following three parameters: number of views M, image matrix size N and s_{FWHM} of the post-smoothing (see table 1). We have developed the method to determine the optimum β_0 from the geometrical correlation coefficient $g(\Delta m)$ among LORs by equation (7). However, the evaluation of $g(\Delta m)$ has an ambiguity because equation (7) contains the length L of LOR that may depend on the diameter of the region of interest and on the location of LORs. In addition, we have made many assumptions in deriving the value of β_0. These may be the reasons why we could not obtain the uniform noise propagation in figure 4. Fortunately, however, the performance of DRAMA is not sensitive to the value of β_0 as shown in figure 6, and we have obtained satisfactory results with the ODRP determined by the proposed method using equations (4)–(8).

For given M and N, a free parameter is the FWHM of the post-smoothing s_{FWHM} that balances the signal-to-noise ratio with the spatial resolution. It is interesting to note that, in DRAMA, the structural error SE is nearly independent of s_{FWHM} as shown in table 4. The increase of s_{FWHM} reduces β_0 and T_{u} that matches the low-resolution reconstruction. This is not the case for the conventional RAMLA or OS-EM, in which T_{u} is independent of s_{FWHM}. It should also be noted that s_{FWHM} has to be determined before the iteration starts because it affects the ODRP, although the iteration itself does not include any smoothing process. We expect the usefulness of the FORE + DRAMA combination for 3D PET imaging. We have also confirmed that DRAMA works in the weighted attenuation correction scheme as well as the conventional OS-EM.

We have applied the same approach to the conventional OS-EM. The dynamic OS-EM (DOSEM) can be operated with a larger OS level without losing the signal-to-noise ratio. DRAMA is a special case of DOSEM where $M_{\text{sub}} = M$, and it is no longer more profitable to use DOSEM with a smaller M_{sub} ($<M$), because DRAMA provides similar performance with

the fastest convergence and smallest computer burden. We have described the application of DRAMA and DOSEM in the 2D image reconstruction in this paper, but the methods will be widely applied to 3D reconstruction problem with some modifications. The concept of dynamic relaxation will also be applied to other block-iterative algorithms such as OS-GP.

Another important application of DRAMA is the reconstruction of SPECT images with non-uniform attenuation media. We have performed preliminary simulation studies under the similar condition to that used in '4.4 attenuation correction', except that the attenuation coefficient was 0.15 cm^{-1} and the number of projection views was 256 in 4π angle (image matrix is 128×128). Two conjugate projections in opposite directions were processed simultaneously as the same LOR, and the apparent number of views was then 128 in 2π angle as in the case of PET. The result showed that two iterations ($\gamma = 0$) with DRAMA provide a satisfactory image ($N_{\mathrm{RMS}} = 9.02\%$, uniformity $= 0.261\%$), which is comparable to that after 16 iterations (OS level $= 8$) with OS-EM ($N_{\mathrm{RMS}} = 9.09\%$, uniformity $= 0.141\%$). The application to the SPECT is beyond the scope of this paper, and the details will be reported elsewhere.

Appendix A

The analysis of the noise propagation is as follows. First, we modified equation (1.2) in an approximate form suitable to the following analysis:

$$x_j^{(k,q+1)} = x_j^{(k,q)} + \lambda_k(q) x_j^{(\mathrm{true})} \frac{a_{ij}}{C_j} \left\{ \frac{y_i - \sum_j x_j^{(k,q)} a_{ij}}{y_i^{(\mathrm{true})}} \right\}. \tag{A.1}$$

We then performed the analysis in the following steps. The subscripts 1 and 2 refer to LOR-1 and LOR-2, respectively.

Step 1. Assume a true image $x_j^{(\mathrm{true})}$ as the initial image of the iteration.
Step 2. Access the noisy projection $y_1 = y_1^{(\mathrm{true})} + e$ along LOR-1, where e denotes the noise component. The error density in the image after accessing y_1 is given by $\lambda_1 a_{1j} e x_j^{(\mathrm{true})} / \left(C_j y_1^{(\mathrm{true})}\right)$.
Step 3. Access the noiseless projection $y_2 = y_2^{(\mathrm{true})}$ along LOR-2, and estimate the corrected image $x_j = x_j^{(\mathrm{true})} + n_j$, where n_j is the noise component. The noise component n_j is given by

$$n_j = \lambda_1 e \frac{x_j^{(\mathrm{true})}}{C_j\, y_1^{(\mathrm{true})}} \left\{ a_{1j} - \lambda_2 a_{2j} \frac{\bar{g}_{12}}{y_2^{(\mathrm{true})}} \right\} \tag{A.2}$$

where

$$\bar{g}_{mn} = \sum\nolimits_j \left(a_{mj} a_{nj} x_j^{(true)} / C_j \right) \qquad (m = 1 \text{ or } 2, n = 1 \text{ or } 2). \tag{A.3}$$

The parameter $\bar{g}_{mn}$ represents the correlation coefficient between $y_m^{(\mathrm{true})}$ and $y_n^{(\mathrm{true})}$.
Step 4. Estimate the total noise in LOR-1 $e^* = \sum_j a_{1j} n_j$, and calculate the ratio $r = e^*/e$, the reduction factor of noise by accessing y_2. Using $\bar{g}_{mn}$ defined by equation (A.3), the noise reduction factor r can be expressed as

$$r = \lambda_1 \frac{\bar{g}_{11}}{y_1^{(\mathrm{true})}} \left\{ 1 - \lambda_2 \frac{\bar{g}_{22}}{y_2^{(\mathrm{true})}} \frac{\bar{g}_{12}\bar{g}_{12}}{\bar{g}_{11}\bar{g}_{22}} \right\}. \tag{A.4}$$

If we assume that $\bar{g}_{11} \approx y_1^{(\mathrm{true})}$, $\bar{g}_{22} \approx y_2^{(\mathrm{true})}$ and $x_j^{(\mathrm{true})} / C_j \approx$ constant, equation (A.4) is reduced to

$$r \approx \lambda_1 \left(1 - \lambda_2\, g_{12}^2\right) \tag{A.5}$$

where

$$g_{12} = \sum_j a_{1j}a_{2j} \Big/ \left(\sum_j a_{1j}^2 \sum_j a_{2j}^2\right)^{1/2}. \tag{A.6}$$

The above assumption is approximately valid for a uniform disc source when the rows of the system matrix are normalized. The parameter g_{12} is the same as the geometrical correlation coefficient between LOR-1 and LOR-2 defined by equation (3).

Appendix B

The derivation of equation (7) is as follows. Consider a simplified model shown in figure 1, where we assume that two LORs cross at the origin of coordinates. The angle between the two LORs is $2\theta(0 \leqslant \theta \leqslant \pi/2)$, where $\theta = \pi\Delta m/(2M)$. We assume that the LORs have a cross-sectional response represented by a Gaussian function, the standard deviation being σ. For $0 \leqslant \Delta m \leqslant M/2(0 \leqslant \theta \leqslant \pi/4)$, the geometrical correlation coefficient of the two LORs is then given by

$$\begin{aligned} g(\Delta m) &= c\int_0^{L/2}\int_{-\infty}^{+\infty} \exp\left\{-\frac{(\xi_\theta - \xi)^2}{2\sigma_\theta^2}\right\}\exp\left\{-\frac{(\xi_\theta + \xi)^2}{2\sigma_\theta{}^2}\right\}\,\mathrm{d}\xi\,\mathrm{d}\psi \\ &\qquad \xi_\theta = \psi\tan\theta, \quad \sigma_\theta = \sigma/\cos\theta \\ &= c\int_0^{L/2}\exp\{-(\xi_\theta/\sigma_\theta)^2\}\int_{-\infty}^{+\infty}\exp\{-(\xi/\sigma_\theta)^2\}\,\mathrm{d}\xi\,\mathrm{d}\psi \\ &= c\,\frac{\sqrt{\pi}\sigma}{\cos\theta}\int_0^{L/2}\exp\left\{-\frac{(\psi\sin\theta)^2}{\sigma^2}\right\}\mathrm{d}\psi \end{aligned} \tag{A.7}$$

where c is a normalization constant. Letting $g(0) = 1$ when $\theta = 0$ in equation (A.7), we obtain $c = 2/(\sqrt{\pi}\sigma L)$. Then we have equation (7.1), from equation (A.7). When $\sin\theta > 3\sqrt{2}\sigma/L$, we can execute the integration in equation (7.1) to obtain equation (7.2). By the symmetry, $g(\Delta m)$ for $M/2 < \Delta m \leqslant M - 1$ is given by equation (7.3). In the above derivation, we have assumed that the two LORs cross at the origin of coordinates, but the equations will hold for any two LORs that cross each other at an angle 2θ.

References

Ahn S and Fessler J A 2001 Globally convergent ordered subsets algorithms: application to tomography *2001 IEEE Nucl. Sci. Symp. and Med. Imaging Conf. Rec.*

Browne J and De Pierro A 1996 A row-action alternative to the EM algorithm for maximizing likelihoods in emission tomography *IEEE Trans. Med. Imaging* **15** 687–99

Comtat C, Kinahan P E, Defrise M, Michel C and Townsend D W 1998 Fast reconstruction of 3D PET data with accurate statistical modeling *IEEE Trans. Nucl. Sci.* **45** 1083–9

Daube-Witherspoon M E, Matej S, Karp J S and Lewitt R M 2001 Application of the row action maximum likelihood algorithm with spherical basis functions to clinical PET imaging *IEEE Trans. Nucl. Sci.* **48** 24–30

Defrise M 1995 A factorization method for the 3D x-ray transform *Inverse Problems* **11** 983–94

De Pierro A R and Yamagishi M E B 2001 Fast EM-like methods for maximum *a posteriori* estimates in emission tomography *IEEE Trans. Med. Imaging* **20** 280–8

Green P J 1990 Bayesian reconstruction from emission tomography data using a modified EM algorithm *IEEE Trans. Med. Imaging* **9** 84–93

Guan H and Gordon R 1994 A projection access order for speedy convergence of ART (algebraic reconstruction technique): a multilevel scheme for computed tomography *Phys. Med. Biol.* **39** 2005–22

Hebert T and Leahy R 1989 A generalized EM algorithm for 3D Bayesian reconstruction from Poisson data using Gibbs priors *IEEE Trans. Med. Imaging* **8** 194–202

Herman G T and Meyer L B 1993 Algebraic reconstruction techniques can be made computationally efficient *IEEE Trans. Med. Imaging* **12** 600–9

Hsiao I-T, Rangarajan A and Gindi G 2002a A probably convergent OS-EM like reconstruction algorithm for emission tomography *Proc. 2002 SPIE Medical Imaging Conference*

Hsiao I-T, Rangarajan A and Gindi G 2002b A new convergent map reconstruction algorithm for emission tomography using ordered subsets and separable surrogates *Proc. 2002 IEEE Int. Conf. on Biomedical Imaging (Washington, DC, July, 2002)*

Hudson H M and Larkin R S 1994 Accelerated image reconstruction using ordered subsets of projection data *IEEE Trans. Med. Imaging* **13** 601–9

Kudo H, Nakazawa H and Saito T 1999 Convergent block-iterative method for general convex cost functions *Proc. 1999 Int. Meeting on Fully Three-Dimensional Image Reconstruction in Radiology and Nuclear Medicine* pp 247–50

Kudo H, Nakazawa H and Saito T 2000 Block-gradient method for image reconstruction in emission tomography *Trans. Inst. Electron. Inf. Commun. Eng. Japan* **J83-D-II** 63–73

Levitan E and Herman G T 1987 A maximum *a posteriori* probability expectation maximization algorithm for image reconstruction in emission tomography *IEEE Trans. Med. Imaging* **6** 185–92

Matej S and Browne J A 1996 Performance of a fast maximum likelihood algorithm for fully 3D PET reconstruction *Three-Dimensional Image Reconstruction in Radiology and Nuclear Medicine* ed P Grangeat and J L Amans (Dordrecht: Kluwer) pp 297–315

Matej S, Daube-Witherspoon M E and Karp J S 2000 Performance of 3D RAMLA with smooth bases function on fully 3D PET data *Proc. 1999 Int. Meeting on Fully Three-Dimensional Image Reconstruction in Radiology and Nuclear Medicine* pp 39–42

Meikle S R, Hutton B F, Bailey D L, Hooper P K and Fulham M J 1994 Accelerated EM reconstruction in total-body PET: potential for improving tumour detectability *Phys. Med. Biol.* **39** 1689–704

Obi T, Matej S, Lewitt R M and Herman G T 2000 2.5-D simultaneous multislice reconstruction by series expansion methods from Fourier-rebinned PET data *IEEE Trans. Med. Imaging* **19** 474–84

Ogawa K and Urabe H 2000 Image quality in the modified ordered subset-Bayesian reconstruction *1999 IEEE Nucl. Sci. Symp. and Med. Imaging Conf. Rec.*

Shepp L A and Vardi Y 1982 Maximum likelihood reconstruction for emission tomography *IEEE Trans. Med. Imaging* **1** 113–22

Snyder D L and Miller M I 1985 The use of sieves to stabilized images produced with the EM algorithm for emission tomography *IEEE Trans. Nucl. Sci.* **32** 3864–72

Tanaka E 1987 A fast reconstruction algorithm for stationary positron emission tomography based on a modified EM algorithm *IEEE Trans. Med. Imaging* **6** 98–105

Xuan L, Comtat C, Michel C, Kinahan P, Defrise M and Townsend D 2001 Comparison of 3D reconstruction with 3D-OSEM and with FORE + OS-EM for PET *IEEE Trans. Med. Imaging* **20** 804–14